

# Development of a Fast Visible Light Measurement System for the Study of Ion Cyclotron Range of Frequency Waves in GAMMA 10/PDX Plasmas

Akira EJIRI, Mafumi HIRATA<sup>1)</sup>, Makoto ICHIMURA<sup>1)</sup>, Masayuki YOSHIKAWA<sup>1)</sup>, Ryuya IKEZOE<sup>2)</sup> and Shuji KAMIO<sup>3)</sup>

*The University of Tokyo, Kashiwa 277-8561, Japan*

<sup>1)</sup>*University of Tsukuba, Tsukuba 305-8577, Japan*

<sup>2)</sup>*Kyushu University, Kasuga 816-8580, Japan*

<sup>3)</sup>*National Institute for Fusion Science, Toki 509-5292, Japan*

(Received 16 July 2021 / Accepted 22 August 2021)

A fast visible light measurement system was installed on GAMMA 10/PDX to measure plasma light fluctuations induced by ion cyclotron range of frequency (ICRF) (6360 kHz) waves. Time evolution and power spectrum were obtained and the relative amplitude of the fluctuations was the order of 0.1%. The difference of measured wavelength region was investigated by using three interference filters, but obtained time evolutions and the relative amplitudes were similar when we neglect a factor of difference. The RF pick-up noise is about two orders of magnitude smaller than the ICRF wave induced plasma signal, and the broad frequency band component is about an order of magnitude smaller than the signal. The latter arises from the shot-noise of the photon detection Poisson process, and an expression of the shot-noise, in which the effects of the frequency response of the system and the detector property are included, was obtained. The expression is confirmed experimentally using a stable light source.

© 2021 The Japan Society of Plasma Science and Nuclear Fusion Research

Keywords: visible light measurement, ICRF, RF measurement, mirror device, Poisson process

DOI: 10.1585/pfr.16.1402096

## 1. Introduction

Ion cyclotron range of frequency (ICRF) heating is a main tool for steady state operation experiments in the present fusion devices. The heating efficiency, however, is not always high enough, and the non-absorbed power, which may be deposited in the SOL plasma near the antenna, would pose a serious problem for steady state operation. While power deposition profiles are calculated by various codes, their accuracies are affected by many practical factors in experiments. In such a situation, internal wave field measurements and comparison of the measured data and the code results are quite important. Such a measurement can be provided by two schemes: one is microwave reflectometry and the other is the plasma light measurement. The former measures the electron density fluctuations induced by RF electric fields [1, 2], and the method was used in several fusion devices such as DIII-D [3, 4], GAMMA 10 [5, 6], TST-2 [7, 8] and LHD [2, 9]. The advantage of microwave reflectometry is its high sensitivity, and the relative density fluctuations down to about  $10^{-5}$  was measured in LHD [2].

The plasma light measurement method can be divided into the following two classes. One is the dynamic Stark-

effect spectroscopy [10, 11], which extracts electric field from the deformation of spectral shape. The deformation is a function of RF frequency and electric field strength [12], and the method can be applied to high frequency waves (e.g. 3.7 GHz in Ref. [10]) because the wavelength shift is proportional to the RF frequency.

The other is the measurements of plasma light intensity fluctuations. In the case of bremsstrahlung, the intensity is proportional to the electron density. In the case of line radiation, the intensity is usually proportional to the electron impact excitation, which is proportional to the electron density. Thus, the intensity is proportional to the electron density, but note that the dependence becomes square of it when the ion density is proportional to the electron density. The measurement principle is the same as that of the microwave reflectometry.

The measurement in visible range is attractive because of good accessibility and availability of various components. In addition, the number of detected photons are expected to be a weak function of the photon energy as shown later. The method was applied to the high harmonic fast waves (with the frequency of 21 MHz) in TST-2 using a photodiode [13] and a photomultiplier tube (PMT) [14]. Comparing these two results, a photodiode is more sensitive to RF pick-up noise, and a PMT seems to be suitable

author's e-mail: ejiri@k.u-tokyo.ac.jp

for ICRF wave measurements.

Measurements of plasma light fluctuations induced by ICRF is not yet established, partly because of the huge noise from the high power ICRF waves, and partly because of the high frequency and small amplitudes. The target frequencies are about an order of magnitude higher than those of recent beam emission spectroscopy [15]. In addition, the difference of the continuous bremsstrahlung measurements and various line radiation measurements have not been compared. The choice of a line or bremsstrahlung would become important at ICRF, because lines have a finite life time, which is the inverse of transition probability, and the order of the life times is 10 - 100 ns for typical visible lines. These finite life times have a function of a low-pass filter, and the frequency response could be deteriorated. In the case of GAMMA 10, the density is relatively low (e.g.,  $2 \times 10^{18} \text{ m}^{-3}$ ) and the number of photons may not be sufficient, because the light intensities are expected to be proportional to the 1st or 2nd power of density. For the case of bremsstrahlung, the number of photons at the energy  $E \sim E + dE$  is proportional to  $n_e^2 Z_{eff} e^{-E/kT_e} dE/E$ , and the photon numbers in soft X-ray and visible light measurements are similar as long as  $dE/E$ s are similar. In GAMMA 10, visible light fluctuation measurement have been carried out and instabilities with several tens kHz were observed [16], but we were not sure whether we can observe the ICRF wave induced visible light fluctuations with much higher frequency and with much smaller amplitude of around 0.1% [17]. The objectives of the present study are the detection of the ICRF wave induced visible light emission in GAMMA 10, and the comparison of choices of different line, and the clarification of the noise source. The paper is organized as follows. The measurement system is described in Sec. 2, and measurement results are shown in Sec. 3. Discussion of the noise is given in Sec. 4. Finally, conclusions are presented in Sec. 5.

## 2. Measurement System

We have developed a fast visible light measurement system and installed it on the GAMMA 10/PDX tandem mirror device to measure the RF induced light intensity fluctuations. The measurement system consists of optics, and two sets of a detector, a preamplifier, a high-pass filter (Fig. 1). An oscilloscope is used to record the signals. The plasma light is collected by a convex lens and made parallel by a concave lens. Three interference filters with the pass-bands of  $375 \pm 5 \text{ nm}$  (OIII and FeI),  $467 \pm 5 \text{ nm}$  (CIII) and  $543 \pm 5 \text{ nm}$  can be used to choose spectral lines. The last filter is used to measure the wavelength range with no apparent spectral line. The light with the last filter is presumably bremsstrahlung. The light passing through the filter is focused on one end of a liquid light guide. The other end is attached to a PMT (Hamamatsu photonics, H10721-110), and the signal is amplified by a two stage amplifier.

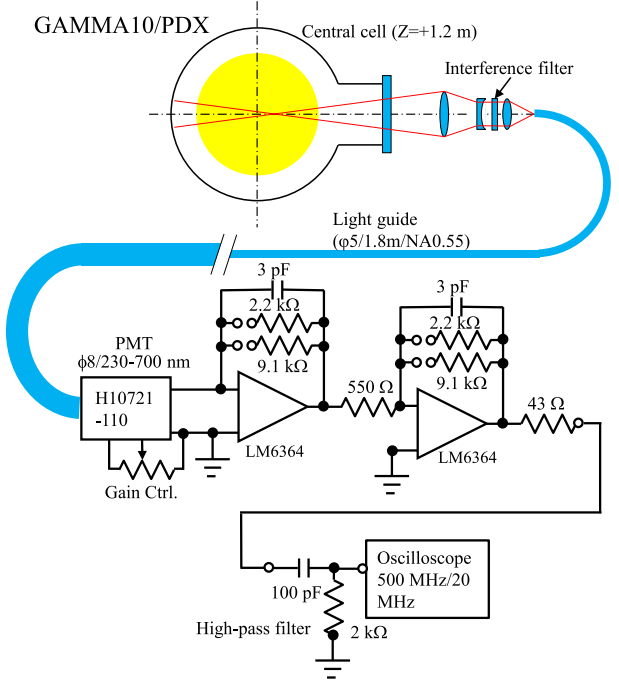


Fig. 1 Schematic drawing of the system composed of optics, a detector, an amplifier, a high-pass filter and an oscilloscope.

The wavelength range (with sensitivity  $> 1/10$  of the maximum) of the PMT is 250 - 640 nm. The output signal of the amplifier is recorded by an oscilloscope. We use a high-pass filter with the cutoff frequency of 800 kHz when we measured the high frequency ICRF induced components to reduce the bit noise. We remove the high-pass filter when we measure the DC and slow components. Two sets of a light guide, a PMT, an amplifier are prepared, and one set is used to measure the plasma light, while the light guide of the other set is covered by a sheet of black-out paper to cut the plasma light and to measure only the RF pick-up noise. Hereafter, these two signals are denoted by plasma channel and shielded channel, respectively. Preparing an additional set cutting the plasma light is quite important to evaluate the RF pick-up noise, because the pick-up noise is often the dominant noise in the measurement. In order to reduce the RF pick-up noise, the PMTs and amplifiers are contained in an diecast aluminium box and DC powers are introduced using feed-through capacitors. The gain of the PMTs is adjusted to a level so that the signal is high enough to avoid the circuit noise effect and low enough to assure the linearity of the system.

Since the target ICRFs were 6360, 9900 and 10300 kHz, a fast response amplifier was developed. The frequency response of the system is measured using a fast response diode laser (Sanyo Semicon Device, DL3247-165), and the results are calibrated using a fast PIN photodiode (Hamamatsu photonics, S8664-02). Figure 2 shows the obtained frequency response of a set of a PMT and

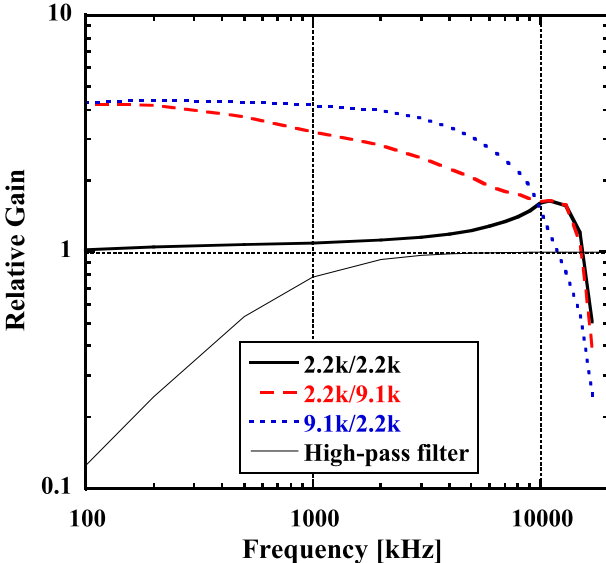


Fig. 2 Frequency response (i.e., gain) of the system with different amplifier resistance combinations and the response of the high-pass filter. The response of the system is measured by using a laser diode as the source, and the response is normalized by the value at 100 kHz with the resistance combination (2.2 kΩ, 2.2 kΩ). The response of the high-pass filter is also plotted.

an amplifier with different combinations of resistances. The response of the high-pass filter is also plotted. The combination of the resistance was selected depending on the target frequencies. In practice, measurements of the higher frequency components 9900 and 10300 kHz showed a small amplitude or a poor signal-noise ratio, and we will show only the measurement results of 6360 kHz in this paper. The wave with this frequency is used to heat the plasma in the central cell.

### 3. Measurement Results

The system was located near a window at  $Z = +1.2$  m (in the central cell) of the GAMMA 10/PDX device. Here,  $Z$  represents the coordinate along the axis of the mirror device, and  $Z > 0$  for the west side. Figure 3 shows the time evolutions of the diamagnetic flux and the line integrated density at the central cell and the plasma light signal measured by our system. The plasma is sustained by ICRF heating with the frequencies of 6360, 9900 and 10300 kHz, and the net injected powers are about 95, 35, 20 kW, respectively. With the increase in density, the plasma light intensity also increases. The amplitude of the high frequency components shows a similar time evolution, while the shielded signal seems to be independent of the discharge (Fig. 3(c)). The ICRF induced plasma signal is extracted from the raw signal and plotted in Fig. 3(d). The extraction method is described later. The ICRF induced signal always becomes large during the initial ramp-up phase of the diamagnetic flux (at  $t \sim 80$  ms). Such be-

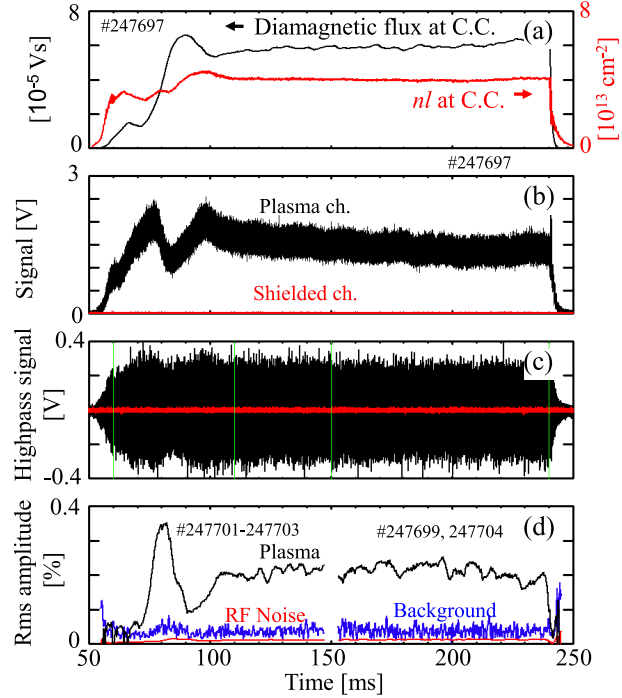


Fig. 3 Time evolution of the diamagnetic flux and the line integrated density at the central cell (a), measured plasma light signal without the high-pass filter (b) and that with the filter (c) and extracted ICRF components (d). Black and red curves in (b) and (c) represents the signals with plasma light and without plasma light (i.e., shielded), respectively. The vertical lines in (c) represent the time windows to calculate power spectra. An interference filter ( $375 \pm 5$  nm) is used. Due to the limited memory size, either the first half or the last half of a discharge can be measured during a discharge.

havior appeared in a past microwave reflectometer signal (Fig. 4 in Ref. [18]). This is possibly related to the appearance of Alfvén ion cyclotron modes accompanied by electron heating [19].

Figure 4 shows the power spectral densities of the plasma channel and the shielded channel. The spectrum of the shielded channel is broad and frequency dependence is very weak. In addition to the broad component, the spectrum shows three peaks at the ICRFs (red arrows in Fig. 4(a)). These peaks represent the RF pick-up noise. The plasma channel spectrum is about one to two orders of magnitude larger than the shielded channel spectrum (Fig. 4(a)) when we neglect fine structures, such as the RF pick-up noise. The high frequency ( $> 100$  kHz) broad component of the plasma channel is well represented by the frequency response of the system with the filter (light blue dashed curve) if the response is multiplied by an appropriate factor. At the ICRF of 6360 kHz, the plasma channel shows about two orders of magnitude larger power than the shielded channel. The peak ratio in Fig. 4(c) is 340, and the ratio between the black and red rms amplitudes in Fig. 3(d) is 18. However, the main noise source

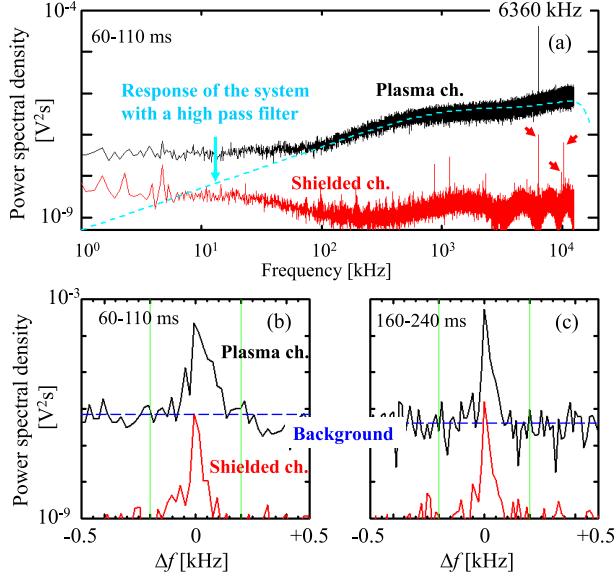


Fig. 4 Power spectral density of the plasma channel and shielded channel. Spectra with a wide frequency range (a), and those with a narrow frequency range (b) and (c) are shown. (a) and (b) are the spectra of the initial ramp-up phase of a discharge, while (c) is those of a quasi stationary phase. An interference filter ( $375 \pm 5$  nm) is used. Frequency response of the system with a high-pass filter is plotted in (a), where an appropriate factor is multiplied to express the broad component by the frequency response. Frequency smoothing of 10 points (0.2 kHz) is applied in (a).

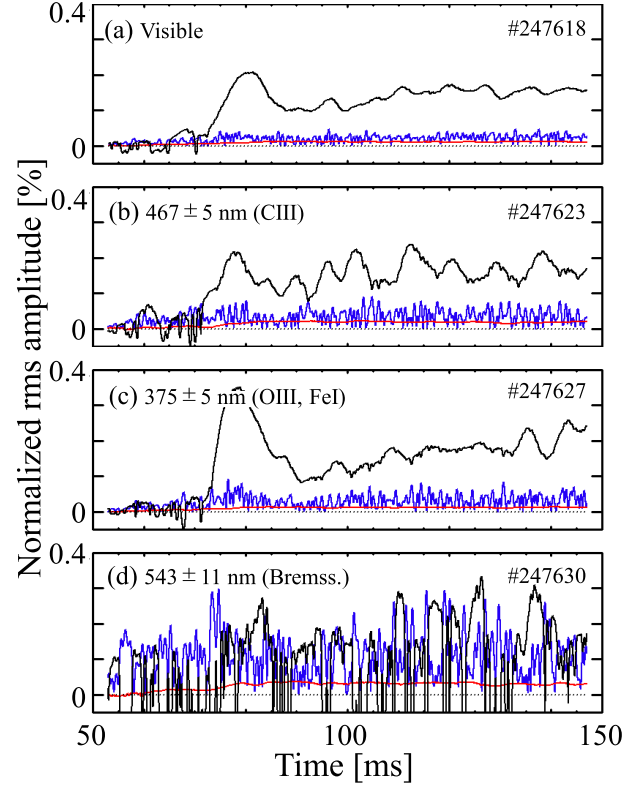


Fig. 5 Time evolutions of extracted ICRF components (black), background components (blue) and RF noise components (red) with or without an interference filter. (a): without a filter, (b)  $467 \pm 5$  nm(CIII), (c)  $375 \pm 5$  nm(OIII, FeI), (d)  $543 \pm 11$  nm(Bremss.).

determining the signal to noise ratio is the background broad component of the plasma channel (approximated by blue dashed lines in Figs. 4(b) and (c)). We will discuss the origin of this broad component, and show that it arises from the photon-noise (i.e., shot noise) affected by the frequency response of the system with a high-pass filter. A narrow band frequency filter of  $6360 \pm 0.2$  kHz (green vertical lines in Figs. 4(b) and (c)) is used to extract the RF components around 6360 kHz, and the rms amplitudes for the plasma channel and the shielded channel are shown in Fig. 3(d). The rms amplitude of the background broad component at  $6360 \pm 0.2$  kHz is speculated from the power spectral density outside the band. In order to obtain the net ICRF induced rms amplitude, the contributions of the RF pick-up noise (red) and the background (blue) are subtracted from that of the plasma channel. Note that the relative rms amplitudes, which are normalized by the slow component (Fig. 3(b)), are plotted in Fig. 3(d), and the typical relative amplitude is the order of 0.1%. Since the past reflectometer measurements showed that the relative amplitudes are less than about 0.5% (in Fig. 5 in [17] and Fig. 4 in [18]), the present results are not inconsistent with the past results. Except for the initial and final phase of a discharge, where the plasma light is weak, the effect of the background is small, and the effect of RF noise is negligi-

ble.

Figure 5 shows the time traces of the extracted components with or without an interference filter. While the measurement with an interference filter of  $543 \pm 11$  nm (Bremss.) failed due to the large background component, the other measurements show similar time evolutions with a similar relative amplitude, if we neglect the difference of a factor of about two. In GAMMA 10/PDX plasmas, CIII, OIII and H $\beta$  lines are dominant lines in the sensitive wavelength range of the system. The life times of their excited states are 14, 10 and 120 ns, respectively, and the life times for CIII, OIII are negligible compared to the period of the ICRF (6360 kHz). The results shown in Figs. 5(b) and (c) are not inconsistent with this expectation. Note that bremsstrahlung is expected to show no time delay from (i.e., fast response to) the density change.

## 4. Discussion of the Noise

The observed relative rms amplitude of ICRF induced plasma light is the order of 0.1% as shown in Fig. 3. However, to measure smaller amplitude or to measure the detailed frequency broadening profile (e.g., Figs. 4(b), (c)), it is necessary to suppress the background broad component. The broad component seems to reflect the frequency

response of the system (Fig. 4(a)). In this section, we estimate the shot-noise arising from the Poisson process of detection, and derive an analytical expression of its power spectrum. In addition, we will demonstrate the agreement between the expression and the measured results. It is well known that the shot-noise causes fluctuations of the detected photon number, which is about  $\sqrt{N}$  when the ensemble average photon number is  $N$ , and such a feature is used to estimate the noise or used in analysis [20, 21]. However, an accurate comparison of the predicted and the measured noise power spectra for a certain system is necessary to determine the performance limits of the system.

In order to measure the photon number  $N$  and its fluctuation, we use an LED as a source and use the same detection system as that used in the plasma measurement. Firstly, the intensity of the LED is adjusted to be sufficiently weak, so that each photon detection signal becomes clear. The statistical features, such as the average time integrated signal intensities are obtained. In addition, several analytical expressions are derived. Secondly, the intensity of the LED is increased, and the measured and the predicted power spectra are compared.

Figure 6 (a) shows the ensemble averaged one photon signal without the high-pass filter (defined as  $\langle y_1(t) \rangle$ ) and the signal with the high-pass filter (defined as  $\langle y_{1hp}(t) \rangle$ ). The shape of the pulse, which reflects the frequency response of the system, is stable and the FWHM pulse width of  $\langle y_1(t) \rangle$  is about 40 ns. The time integral of this signal is used to estimate the photon number for a given signal. When we measure an intense signal  $v(t)$  during a period of  $T$ , the ensemble averaged photon number is written as

$$\langle N \rangle = \frac{\int_0^T \langle v(t) \rangle dt}{\int \langle y_1(t) \rangle dt}. \quad (1)$$

Hereafter, we assume that  $N$  is large enough that the difference between  $N$  and  $\langle N \rangle$  is negligible. This period  $T$  should be that used for the calculation of power spectrum.

Figure 6 (b) shows the distribution of the pulse height obtained from the pulse height analysis of many one photon signals. The distribution is broad and the standard deviation normalized by the average height is defined as  $\sqrt{\langle \tilde{\delta}^2 \rangle}$  ( $= 0.82$  for the present case). Note that the gain of the PMT was increased by more than an order of magnitude from the typical gain for the plasma measurements to reduce the effect of dark currents (i.e., signals with no light). Not only the pulse height distribution shape but also  $\sqrt{\langle \tilde{\delta}^2 \rangle}$  varies with the gain. Each ensemble of one photon signal is written as

$$y_1(t) = \langle y_1(t) \rangle (1 + \tilde{\delta}). \quad (2)$$

Then the signal  $v(t)$  is written as

$$v(t) = \sum_{i=1}^N y_1(t - t_i) = \sum_{i=1}^N \langle y_1(t - t_i) \rangle (1 + \tilde{\delta}_i), \quad (3)$$

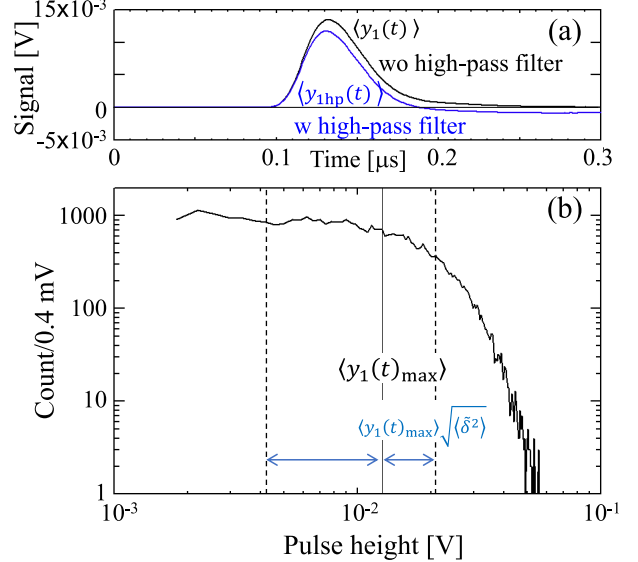


Fig. 6 Time evolutions of the one photon signal with and without a high-pass filter (a), and the distribution of the pulse height (b). Average pulse height  $\langle y_1(t) \rangle_{\text{max}}$  and the region of the standard deviation are shown by vertical lines in (b).

where  $t_i$  denotes the appearance time of a certain one photon signal. In the following, we consider the effect of the high-pass filter. With the filter, the signals  $v(t)$  and  $\langle y_1(t) \rangle$  become  $v_{hp}(t)$  and  $\langle y_{1hp}(t) \rangle$  (the blue curve in Fig. 6 (a)), respectively. We also introduce the Fourier transform of these signals as

$$v_{hp}(t) \xrightarrow{\text{F.T.}} V_{hp}(f), \quad \langle y_{1hp}(t) \rangle \xrightarrow{\text{F.T.}} Y_{hp}(f). \quad (4)$$

We also define  $V(f)$  and  $Y(f)$  in a similar manner. Using Eq. (3),  $V_{hp}(f)$  is written as

$$V_{hp}(f) = \sum_{i=1}^N Y_{hp}(f) e^{-i2\pi f t_i} (1 + \tilde{\delta}_i). \quad (5)$$

The power spectrum becomes

$$\begin{aligned} & V_{hp}(f) V_{hp}^*(f) \\ &= \sum_{i,j}^N Y_{hp}(f) Y_{hp}^*(f) (1 + \tilde{\delta}_i)(1 + \tilde{\delta}_j) e^{-i2\pi f(t_i - t_j)}. \end{aligned} \quad (6)$$

The ensemble averaged power spectrum is written as

$$\begin{aligned} \langle V_{hp}(f) V_{hp}^*(f) \rangle &= \sum_{i,j}^N Y_{hp}(f) Y_{hp}^*(f) \langle (1 + \tilde{\delta}_i)(1 + \tilde{\delta}_j) \rangle \\ &\times \langle e^{-i2\pi f(t_i - t_j)} \rangle. \end{aligned} \quad (7)$$

When we measure a stable DC signal  $\langle v(t) \rangle = \text{const.}$ , then  $t_i$  is randomly and homogeneously distributed over the period  $T$ , and  $\langle e^{-i2\pi f(t_i - t_j)} \rangle = 0$  (for  $i \neq j$  and  $f \neq 0$ ). The power spectrum becomes

$$\langle V_{hp}(f) V_{hp}^*(f) \rangle = \sum_i^N Y_{hp}(f) Y_{hp}^*(f) \left( 1 + \langle \tilde{\delta}^2 \rangle \right) (f \neq 0) \quad (8)$$

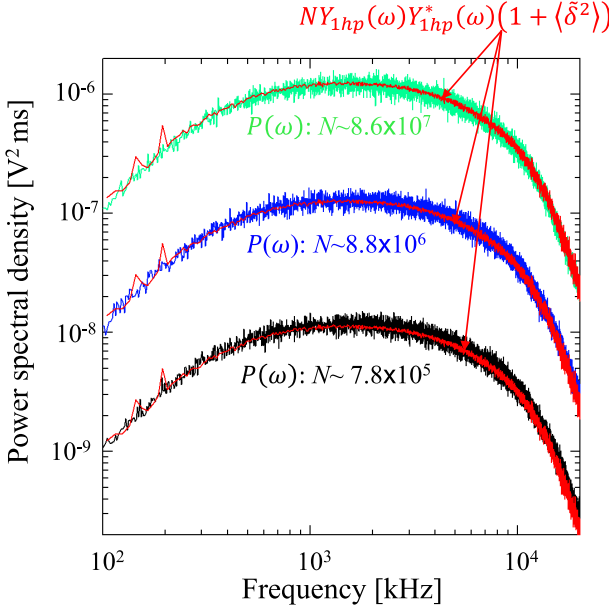


Fig. 7 Comparison of the measured and predicted spectra with different light intensities.

$$= NY_{\text{hp}}(f)Y_{\text{hp}}^*(f)\left(1 + \langle \tilde{\delta}^2 \rangle\right). \quad (8)$$

Here we use the relationship  $\langle(1 + \tilde{\delta}_i)(1 + \tilde{\delta}_j)\rangle = 1 + \langle \tilde{\delta}^2 \rangle$ . The power with nonzero  $f$  represents the shot noise, which is proportional to  $N$ . When  $\langle v(t) \rangle$  has a certain frequency component at  $f = k/T$  ( $k$ : integer), then  $\langle e^{-i2\pi f(t_i - t_j)} \rangle \neq 0$  (for  $t_i - t_j = IT/k$  ( $I$ : integer)), and such a frequency component is added to the power spectrum.

Figure 7 shows the comparison of the measured and predicted spectra for a DC light source with different light intensities. Firstly, signals without the high-pass filter are measured to obtain the photon numbers using Eq. (1). Secondly, signals with the high-pass filter are measured and their power spectra are calculated. The predicted power spectra shown by red curves are obtained using Eq. (8). The agreement demonstrate the correctness of Eq. (8). This expression indicates that the power spectrum is proportional to the frequency response of the system including the high-pass filter, and the level is proportional to the photon number  $N$ . In addition, the level is enhanced by the factor  $1 + \langle \tilde{\delta}^2 \rangle$ .

Here, we derive the signal to noise ratio, assuming that the ICRF induced light fluctuation (in the frequency range of  $f \sim f + \Delta f$ ) has a relative amplitude of  $\varepsilon$  with respect to the DC component (at  $f = 0$ ). The power of the signal becomes  $\varepsilon^2 V(0)V^*(0)\Delta f$ , when we neglect the frequency response of the system. Here,  $\Delta f \equiv 1/T$  is the fundamental frequency (i.e., frequency resolution) in Fourier transform. With the frequency response including the high-pass filter effect, the signal power is written as

$$\varepsilon^2 V(0)V^*(0) \frac{Y_{\text{hp}}(f)Y_{\text{hp}}^*(f)}{Y(0)Y^*(0)} \Delta f. \quad (9)$$

Since  $N = |V(0)|/|Y(0)|$ , the power is rewritten as

$$\varepsilon^2 N^2 Y_{\text{hp}}(f)Y_{\text{hp}}^*(f)\Delta f. \quad (10)$$

The (background) noise power in  $\Delta f$  becomes

$$NY_{\text{hp}}(f)Y_{\text{hp}}^*(f)\left(1 + \langle \tilde{\delta}^2 \rangle\right)\Delta f. \quad (11)$$

Here, we use Eq. (8). Then the signal to noise ratio is written as

$$\frac{\varepsilon^2 N^2 Y_{\text{hp}}(f)Y_{\text{hp}}^*(f)\Delta f}{NY_{\text{hp}}(f)Y_{\text{hp}}^*(f)\left(1 + \langle \tilde{\delta}^2 \rangle\right)\Delta f} = \frac{\varepsilon^2 N}{\left(1 + \langle \tilde{\delta}^2 \rangle\right)} \quad (12)$$

$$= \frac{\varepsilon^2 N}{\left(1 + \langle \tilde{\delta}^2 \rangle\right)\Delta f T}. \quad (13)$$

The last expression indicates that the signal to noise ratio is proportional to the photon count rate  $N/T$  and to the signal power spectral density  $\varepsilon^2/\Delta f$ . These features are quite reasonable, and higher photon count rate (i.e., stronger light intensity) is preferable, and narrower frequency spread structure is easier to detect. Furthermore, the frequency response of the system does not affect the signal to noise ratio as long as the shot-noise is the dominant noise term. It should be noted that the low-pass filter effect due to finite life time of excited states is important, because it could decrease the light fluctuation amplitude  $\varepsilon$  itself for a given density fluctuation amplitude.

## 5. Conclusions

A fast visible light measurement system was fabricated and installed on GAMMA 10/PDX to measure the plasma light fluctuations induced by ICRF waves. The system has two identical channels: one to measure the plasma light and the other to measure the RF pick-up noise. The measured relative amplitude of the ICRF (6360 kHz) induced fluctuations is the order of 0.1%, and it is about two orders of magnitude larger than the RF pick-up noise, and about an order of magnitude larger than the broad frequency band component. The latter arises from the shot-noise of the photon detection Poisson process. We derived a new expression for the shot-noise, in which the effects of the frequency response and the pulse height distribution of an PMT are included. The expression is confirmed experimentally. In order to reduce the shot-noise effect, a larger photon number is preferable, but may not be so easy in low density plasmas. The difference of selected wavelength region was investigated by using three interference filters, but the difference was not so large.

## Acknowledgements

This work is supported by National Institute for Fusion Science Collaboration Research Program NIFS17KUGM125.

- [1] H. Hojo, A. Mase, R. Katsumata, M. Inutake, A. Itakura and M. Ichimura, Jpn. J. Appl. Phys. **32**, 3287 (1993).
- [2] A. Ejiri, T. Tokuzawa, N. Tsujii, K. Saito, T. Seki, H. Kasahara *et al.*, J. Instrumentation **10**, C12032 (2015).
- [3] J.H. Lee, E.J. Doyle, N.C. Luhmann Jr, W.A. Peebles, C.C. Petty, R. Pinsker and T.L. Rhodes, Rev. Sci. Instrum. **68**, 462 (1997).
- [4] J.H. Lee, W.A. Peebles, E.F. Jaeger, E.J. Doyle, N.C. Luhmann Jr, C.C. Petty, R. Pinsker, R. Prater and T.L. Rhodes, Phys. Rev. Lett. **80**, 2330 (1998).
- [5] A. Mase, T. Tokuzawa, N. Oyama, Y. Ito, A. Itakura, H. Hojo, M. Ichimura, M. Inutake and T. Tamano, Rev. Sci. Instrum. **66**, 821 (1995).
- [6] R. Ikezoe, M. Ichimura, T. Okada, J. Itagaki, M. Hirata, S. Sumida *et al.*, Rev. Sci. Instrum. **88**, 033504 (2017).
- [7] T. Yamada, A. Ejiri, Y. Shimada, T. Oosako, J. Tsujimura, Y. Takase and H. Kasahara, Rev. Sci. Instrum. **78**, 083502 (2007).
- [8] T. Oosako, Y. Takase, A. Ejiri, Y. Nagashima, Y. Adachi, H. Kasahara *et al.*, Nucl. Fusion **49**, 065020 (2009).
- [9] A. Ejiri, T. Tokuzawa, K. Saito, T. Seki, H. Kasahara, T. Mutoh, R. Kumazawa, I. Yamada and Y. Takase, in Proceedings of the 12th Asia Pacific Physics Conference (APPC12) (JPS Conf. Proc. **1**), 015038 (2014).
- [10] C.C. Klepper, R.C. Isler, J. Hillairet, E.H. Martin, L. Colas, A. Ekedahl *et al.*, Phys. Rev. Lett. **110**, 215005 (2013).
- [11] E.H. Martin, M. Goniche, C.C. Klepper, J. Hillairet, R.C. Isler, C. Bottereau *et al.*, Plasma Phys. Control. Fusion **57**, 065011 (2015).
- [12] E.H. Martin, C. Lau, M. Brookman and J. Lohr, Rev. Sci. Instrum. **89**, 10D117 (2018).
- [13] Y. Torii, A. Ejiri, T. Masuda, T. Oosako, M. Sasaki, H. Tojo *et al.*, Plasma Fusion Res. **2**, 023 (2007).
- [14] Y. Adachi, A. Ejiri, Y. Takase, O. Watanabe, T. Oosako, H. Tojo *et al.*, Rev. Sci. Instrum. **79**, 10F507 (2008).
- [15] R. Ke, Y.F. Wu, G.R. McKee, Z. Yan, K. Jaehnig *et al.*, Rev. Sci. Instrum. **89**, 10D122 (2018).
- [16] H. Higaki, M. Ichimura, K. Horinouchi, K. Nakagome, S. Kakimoto, Y. Yamaguchi *et al.*, Rev. Sci. Instrum. **75**, 4085 (2004).
- [17] R. Ikezoe, M. Ichimura, J. Itagaki, M. Hirata, S. Sumida, S. Jang *et al.*, J. Instrumentation **12**, C12017 (2017).
- [18] R. Ikezoe, M. Ichimura, J. Itagaki, M. Hirata, S. Sumida, S. Jang *et al.*, AIP Conf. Proc. **1771**, 050002 (2016).
- [19] M. Yoshikawa, R. Ikezoe, K. Ohta, X. Wang, J. Kohagura *et al.*, Plasma Fusion Res. **11**, 2402051 (2016).
- [20] A. Ejiri, T. Oikawa and H. Toyama, Rev. Sci. Instrum. **66**, 4600 (1995).
- [21] A. Ejiri, T. Yamaguchi, J. Hiratsuka, Y. Takase, M. Hasegawa and K. Narihara, Plasma Fusion Res. **5**, S2082 (2010).